ELSEVIER

Ordered arrays of Ni magnetic nanowires: Synthesis and investigation

K.S. Napolskii[a], A.A. Eliseev[a],*, N.V. Yesin[a], A.V. Lukashin[a], Yu. D. Tretyakov[a],
N.A. Grigorieva[b], S.V. Grigoriev[c], H. Eckerlebe[d]

[a]Department of Materials Science, Moscow State University, Moscow 119992, Russia
[b]St-Petersburg State University, St-Petersburg 198504, Russia
[c]Petersburg Nuclear Physics Institute, Gatchina, St-Petersburg 188300, Russia
[d]GKSS Forschungszentrum, Geesthacht 21502, Germany

Available online 31 October 2006

Abstract

The present study is focused on the synthesis and investigation of anodic aluminum oxide (AAO) films and magnetic nanocomposites Ni/AAO obtained by Ni electrodeposition into porous matrix. AAO membranes and magnetic nanocomposites were investigated by HRSEM, EDX microanalysis, XRD, nitrogen capillary adsorption method, SQUID magnetometry, and polarized small-angle neutron scattering (SANS). The influence of synthesis conditions and form factor effect on the magnetic properties of nanowire arrays is reported.
© 2006 Elsevier B.V. All rights reserved.

PACS: 75.75. + a; 75.25. + z; 75.30.Gw; 75.50.Ss

Keywords: Anodic aluminum oxide; Magnetic nanocomposite; Nanowires; Electrodeposition; Polarized small-angle neutron scattering (SANS)

1. Introduction

Anodic aluminum oxide (AAO) membranes formed by two-step anodization technique or nanoimprint technology are well-known to possess uniform pore structure with hexagonal arrangement of cylindrical channels. The use of different electrolytes, voltages and anodic oxidation times allows one to adjust pore diameter D_p, interpore distance D_{int} and film thicknesses L_f in a wide range ($D_p = 5–160$ nm; L_f up to several hundreds of micrometers) [1]. This makes anodic alumina extremely attractive as a matrix or reactor for the synthesis of nanocomposites owing to the possibility of formation of membranes with ultra-high length of mesopores at very low diameters (which could be considered as one dimensional). Besides, incorporation of almost any compound into AAO matrix could be carried out by electrodeposition technique, enabling simple handling over loading values and anisotropy of nanostructures. AAO films have been widely used as solid state nanoreactors for the preparation of metal and metal oxide nanowires, complex inorganic/organic composites, polymer fibers, carbon nanotubes, etc. [1–3].

One of the most important challenges in physics and materials science today is the preparation of ordered nanostructure arrays with controlled properties and dimensions [4]. Thus porous alumina films and nanocomposites based on AAO membranes could be used as perfect model objects for a deeper understanding of processes and unusual effects on nanolevel in spatially ordered systems.

Several works report investigation of organization of mesopore channels formed during anodization process; however, most of them involve only electron microscopy or scanning probe microscopy studies [5–8] which are known for their locality and only a few rely on small-angle scattering techniques for quantitative characterization. Although small-angle neutron scattering (SANS) and small-angle X-ray scattering (SAXS) methods were extensively used for studying spatially ordered materials, a few works have been done for characterization of AAO membranes and AAO-based nanocomposites. In the same time these methods can provide extremely valuable information on pore structure (interpore distance, diameter and length) and organization (spatially correlated volumes,

*Corresponding author. Tel.: +7 495 9395248; fax: +7 495 9390998.
E-mail address: eliseev@inorg.chem.msu.ru (A.A. Eliseev).

AAO domain size). Recently, SAXS was successfully applied for calculation of periodicity parameters of anodic alumina films and determination of loading value and homogeneity of cobalt wires grown in AAO templates [9]. However, the penetration distance of electron irradiation to solid state objects usually equals only a few microns, while characterization of alumina membranes (with thickness sometimes exceeding several hundreds micrometers) requires higher penetration depths, which could be achieved using neutrons instead of X-rays. Therefore in the present work, we performed detailed SANS examination of AAO membranes with different pore diameters. It should also be noted that in case of intercalation of magnetic materials inside the pores, neutron scattering enables us to investigate the magnetic properties of nanocomposites by polarized SANS technique, which allows one to determine magnetic scattering contribution in magnetized samples. The superstructure of the magnetic nanowires of the spatially ordered arrays gives a magnetic field-dependent contribution to the Bragg reflection.

2. Experimental section

2.1. Preparation of porous alumina matrices

AAO membranes were prepared by the two-step anodization technique described elsewhere [1,5–8]. This method allows producing porous films with well-ordered hexagonal arrays of cylindrical channels.

High-purity (99.99%) aluminum foil (0.5 mm thick) was used as the starting material. Before anodization the aluminum was annealed at 550 °C in air in order to remove the mechanical stress and enhance the grain size in the metal. Subsequently, the foils were mechanically polished to a mirror finish and cleaned repeatedly with acetone and deionized water. Copper wires used as current collectors were isolated with silicone seal.

The anodization was carried out in a two-electrode cell in 0.3 M oxalic acid at constant voltage 40 V using Pt foil as a counterelectrode. The electrolyte was rigorously stirred and its temperature was kept in the range of 0–5 °C during anodization. After first anodization for 24 h alumina film was selectively etched away in a mixture of 35 ml/l H_3PO_4 and 20 g/l CrO_3 at 70 °C. After second anodization under the same conditions and oxidation times between 50 and 100 h oxide layers with thicknesses between 90 and 180 μm were obtained. Enlargement of pores diameter was carried out by chemical etching of porous films in 0.3 M oxalic acid at 30 °C for 2.5, 5 and 10 hours. The obtained samples were denoted as AA_0 h (as-prepared sample without pore widening), AA_2.5 h, AA_5 h and AA_10 h.

To separate the oxide film from the substrate the remaining aluminum was dissolved using a solution of 10 vol% Br_2 in methanol at room temperature. Subsequently, the pore bottoms were opened by chemical etching in a mixture of 35 ml/l H_3PO_4 and 20 g/l CrO_3 at 70 °C.

2.2. Preparation of Ni magnetic nanocomposites based on AAO membranes

In order to prepare Ni nanowire arrays by electrodeposition technique, a layer of Au film was sputtered onto one side of the AAO template to serve as the working electrode.

Electrochemical experiments were carried out in a three-electrode cell at room temperature. The counterelectrode was a Pt wire and the reference electrode was a saturated Ag/AgCl electrode connected to the cell via a Luggin capillary. Potentials hereinafter are given versus Ag/AgCl reference electrode ($E_{Ag/AgCl} = 0.199$ V versus standard hydrogen electrode). 20 g/l H_3BO_3, 20 g/l $NiCl_2 \cdot 6H_2O$ and 160 g/l $NiSO_4 \cdot 7H_2O$ solution was used for potentiostatic Ni deposition at $E_d = -0.85$ V. The obtained nanocomposites of Ni/AAO were denoted as AA_th_Ni_l, where t is the pore widening time in 0.3 M $(COOH)_2$ at 30 °C; and l is the calculated length of Ni nanowires in micrometers obtained from several characterization methods (HRSEM, electric charge, saturation magnetization M_s).

2.3. Samples characterization

Anodic alumina films and Ni nanocomposites based on AAO membranes were studied by HRSEM, EDX microanalysis, XRD, nitrogen capillary adsorption method, SQUID magnetometry and polarized SANS. XRD analysis was carried out using DRON 3 M, CuK_α radiation and scan step 0.01–0.05°. The surface properties were characterized with QuantaChrome NOVA 4200E instrument (working gas N_2, 77 K). High-resolution scanning electron microscopy (SEM) and EDX microanalysis were performed using HRSEM LEO Supra 50 VP with microanalytical system INCA Energy + Oxford. The magnetic properties of Ni/AAO nanocomposites were studied with a Cryogenics S-600 SQUID magnetometer.

Polarized SANS measurements were carried out at the SANS-2 setup of Geesthacht Neutron Facility (GeNF). A polarized beam of neutrons with an initial polarization of $P_0 = 0.94$, the neutron wavelength $\lambda = 5.8$ Å ($\Delta\lambda/\lambda = 0.1$) and a divergence of 1.5 m rad was used. An external magnetic field (0–300 mT) was applied in the horizontal plane and perpendicularly to the incident beam.

3. Results and discussion

3.1. Characterization of porous structure of anodic alumina film

In the present work, films with different thicknesses and pore diameters were obtained (pore diameter from 25 to 93 nm; thicknesses from 1 to 150 μm). Film thicknesses were controlled by anodization time and the pore diameter by duration of pore widening in 0.3 M $(COOH)_2$ at 30 °C.

According to the direct HRSEM observation all synthesized samples possess ordered porous structure with uniform pores aligned perpendicular to the film surface (Fig. 1). Besides the pore diameter depends on the etching time: the longer the time of pore widening, the porous structure with larger pore is formed.

To obtain more information about the porous structure of alumina films, the SANS and capillary adsorption of nitrogen at 77 K experiments were carried out. The obtained data are summarized in Table 1.

The q-dependence of the neutron intensity $I(q)$ for pure AAO matrices is shown in Fig. 2. Wide diffraction peaks at $q \sim 0.068$ and 0.12 nm^{-1} were observed in SANS spectra of the films independently of anodization duration, which corresponds to a hexagonal pores structure with $d_{100} = 91.7$ nm and $d_{110} = 53.2$ nm, where $d = 2\pi/q$. Thus, the cell parameter of the structure and the interpore distance are $a = D_{int} = 2d_{110} = 106.4$ nm. It should be noted that pore widening by chemical etching leads to some shift of the diffraction peak to smaller q-values

(larger lattice parameters), which can be interpreted as removing the mechanical stress in thick porous films.

Capillary adsorption of nitrogen on porous alumina membranes at 77 K represented type H4 isotherms (typical for mesoporous solids), indicating the presence of uniform cylindrical pores with diameters depending on the duration of the pore-widening stage. The correlation between experimental and theoretically calculated data is shown in Table 1. According to a theoretical calculation, the specific surface area of the AAO membranes in the assumption of the hexagonal arrangement of cylindrical pores with cell parameter $a = 106$ nm (SANS data) ranges from $S = 3.4$ m^2/g for as-prepared samples with $D_p = 28$ nm (AA_0 h) to 48.9 m^2/g for the sample subjected to 10 h pore widening procedure (AA_10 h). However, experimental values were found to exceed calculated ones several times. That can be explained by nonideality of the anodic alumina films and the presence of micropores in the structure. The pore size distribution plot for AA_0 h sample indicates the presence of one narrow characteristic
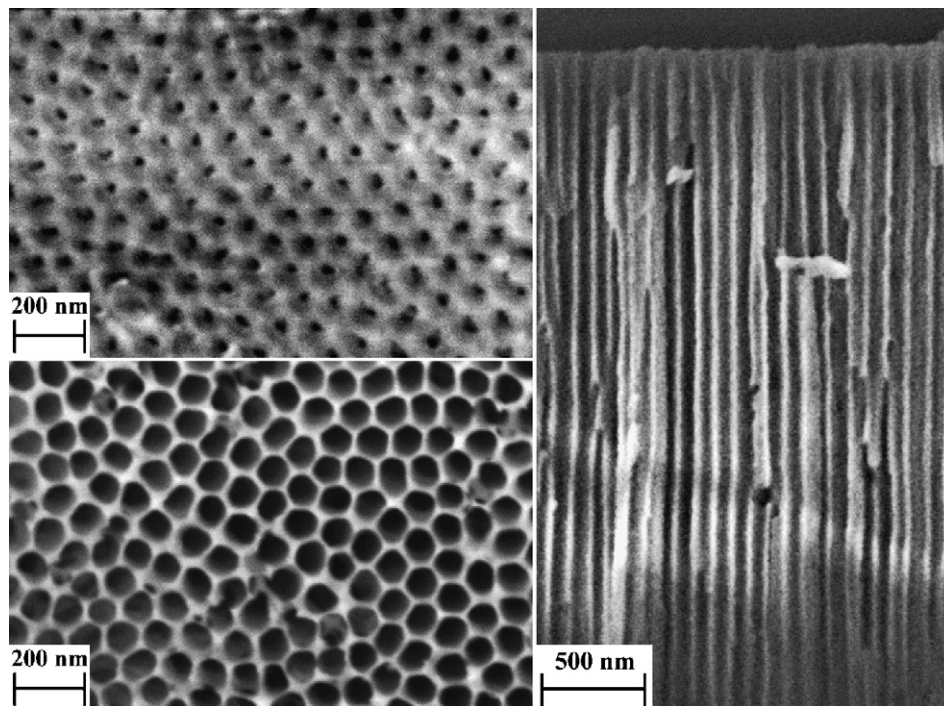

Fig. 1. HRSEM data for AAO membranes: top view of AA_0h (a) and AA_10h (b) samples; cross-sectional image of AA_5h porous film (c).

Table 1
Structure parameters of anodic alumina films

Sample	SEM		SANS	BET	Theoretical calculation	BJH
	D_p(nm)	D_{int} (nm)	D_{int} (nm)	S (m^2/g)	S (m^2/g)	$\langle D_p \rangle$ (nm)
AA_0h	25	105	106.4	10.88	3.4	28
AA_2.5h	49	105		23.36	6.5	46
AA_5h	68	105	110.7	34.78	9.4	58
AA_10h	80	105		132.70	48.9	92

peak at $\langle D_{\mathrm{p}} \rangle = 28$ nm, while for AA_10 h sample two peaks at average diameters of 3 and 92 nm are clearly seen. The first peak originates likely from micropores formed between the channels at long etching times. The second should be obviously ascribed to widening of the initial channels. It is worth noting that the size distribution of pores is relatively narrow for all the matrices and does not depend on the etching time. It indicates uniform widening of the pores throughout their length. These results are in good agreement with the cross-sectional image of AA_5 h porous film (see Fig. 1c).

For homogeneous filling of the porous framework by Ni particles electrodeposition was performed at low potential (-0.85 V versus Ag/AgCl) using a sputtered gold layer as working electrode. Au layer allows one to achieve a high number of active centers for primary nucleation of Ni on the electrode surface, while deposition at low potential enables one to prevent the blocking of narrow pores by H_2 bubbles. The formation of metallic Ni during the electrodeposition step was proved by XRD and EDX studies.
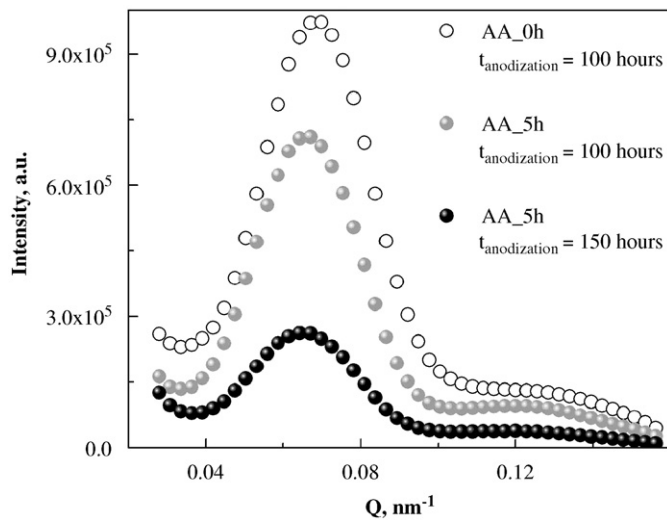
HRSEM of Ni/AAO nanocomposites indicates that Ni particles' shape and diameter are in good agreement with that of the pores, while their length depends directly on duration of electrodeposition. A cross-sectional HRSEM image shows homogeneous filling of the pores by Ni nanowires (Fig. 3a).

The magnetic properties of Ni/Al$_2$O$_3$ nanocomposites were investigated by SQUID magnetometry. The obtained data are summarized in Table 2.

Magnetization reversal curves have a strong dependence of coercivity and remanence magnetization on orientation of the wires in the external magnetic field (Fig. 4). Nanocomposites exhibit large coercivity and remanence in the parallel direction of the field vector towards the wire axis, while perpendicular geometry gives a characteristic decrease of these values, illustrating magnetization in the hard magnetic axis. One should note that magnetization reversal curves in perpendicular orientation indicate a saturation field of Ni/Al$_2$O$_3$ nanocomposites of 3500 Oe, which is very close to theoretically calculated value for Ni nanowires $2\pi M_{\mathrm{s}} = 3050$ Oe [10]. Thus, the obtained data are in good agreement with the curling switching model of anisotropic magnetic particles.

For matrices with small pores diameter (AA_0h_Ni_l series) increasing the particles length results in increase of

Fig. 2. SANS intensity profile from pure AAO matrices.

Table 2
Magnetic characteristics of Ni/AAO nanocomposites

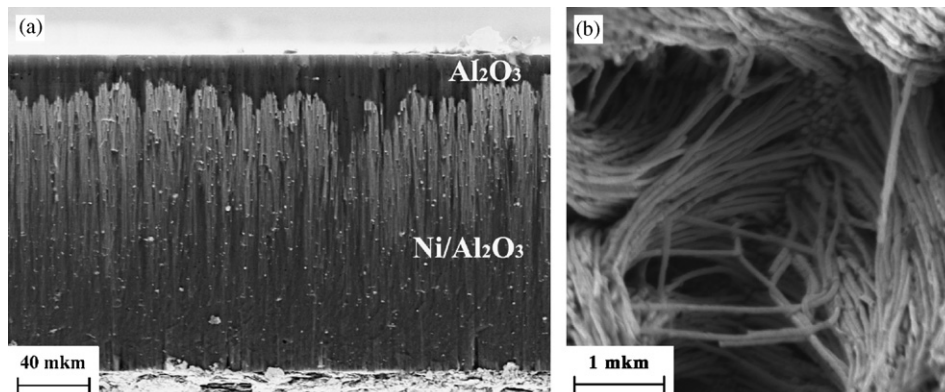| Sample	Particles diameter (nm)	H_{c}, Oe				$M_{\mathrm{r}}/M_{\mathrm{s}}$ (%)			
		4 K		300 K		4 K		300 K	
		$H\|l$	$H\perp l$	$H\|l$	$H\perp l$	$H\|l$	$H\perp l$	$H\|l$	$H\perp l$
AA_0h_Ni_0.064	25	318	209	63	53	10	10	9	7
AA_0h_Ni_1.6	25	519	234	216	64	24	15	27	26
AA_0h_Ni_150	25	664	220	555	191	62	10	65	9
AA_5h_Ni_0.089	70	227	268	75	35	5	10	33	4
AA_5h_Ni_3.4	70	527	74	560	83	27	3	91	4
AA_5h_Ni_50	70	490	160	450	140	44	7	55	8

Fig. 3. HRSEM data for Ni/AAO nanocomposites: cross-sectional image of **AA_0h_Ni_150** sample (a); top view of AA_5h_Ni_50 after dissolution of oxide matrix (b).
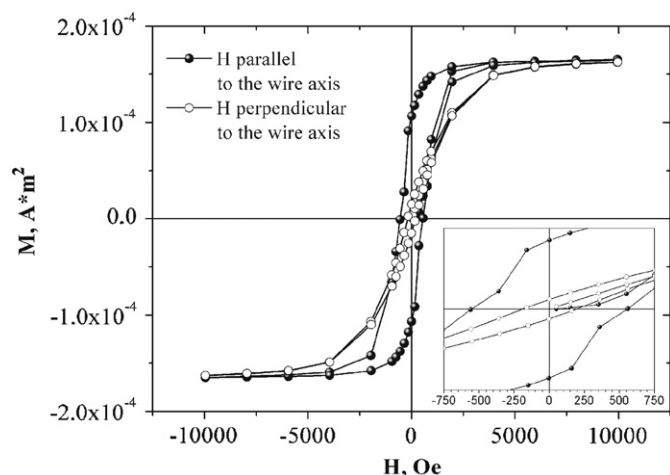
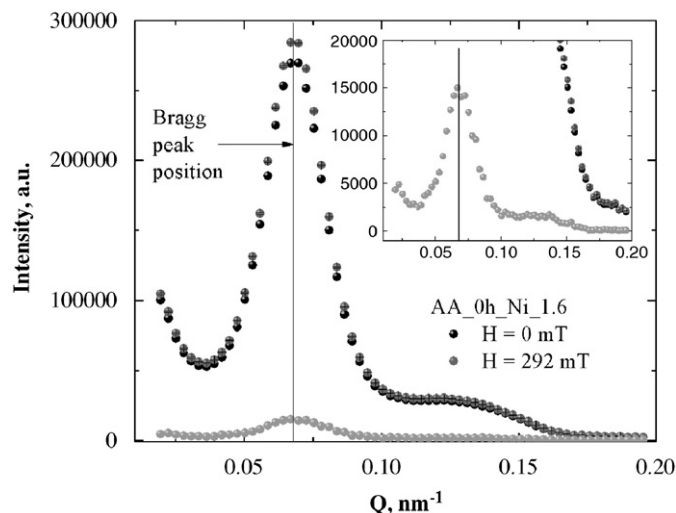Fig. 4. Magnetic hysteresis for AA_0h_Ni_150 nanocomposite.

Fig. 5. The field-reliant q-dependence of the neutron intensity for a nanocomposite AA_0h_Ni_1.6.

coercivity along the magnetic easy axis up to 555 Oe for AA_0h_Ni_150 sample, while the coercivity value in the perpendicular direction remains constant.

In case of Ni nanowires with large diameter (AA_5h_Ni_l series) the dependence of coercivity value along the magnetic easy axis from particles length has a maximum. This could be ascribed to the appearance of strong magnetic dipole interaction between neighboring wires and their assembling to the domain structure.

To determine the correlation between the porous structure of AAO matrix and the magnetic structure of the nanocomposites, polarized SANS experiments have been performed. The cross-section of polarized neutrons consists of a nuclear contribution (depending on nuclear density and their cross-section), a magnetic part (depending on the density and the orientation of the magnetic moments of the atoms towards scattering vector) and a nuclear–magnetic interference of the scattering. As nickel nanowires are ferromagnetic, they could be ordered by the applied magnetic field while nuclear contribution is not affected by the external field. Polarized SANS studies enable us to investigate pure magnetic scattering and exactly determine ordering parameters of spatially ordered magnetic phases.

The field-reliant q-dependence of the neutron intensity $I(q)$ for a nanocomposite AA_0h_Ni_1.6 is shown in Fig. 5. It is clearly seen that applying the external magnetic field induces a noticeable increase of the diffraction peak intensity. The inset in Fig. 5 shows the value of the field-dependent part of neutron scattering ($I_H(q) = I(q,H) - I(q,0)$) as a function of q. The coincidence of Bragg's peak position at $q \sim 0.068\,\text{nm}^{-1}$ for nuclear scattering (at zero magnetic field) with the maximum of the magnetic scattering from AA_0h_Ni_1.6 sample confirms the formation of the spatially ordered magnetic structure, e.g. 1 D nanowire array with periodicity of 106.4 nm.

Thus the use of SANS technique with variable magnetic field gives us a unique tool for studying spatially ordered

magnetic systems and enables us to determine their magnetic properties at any length scales excluding non-homogeniety effects and defects of microstructure.

4. Conclusions

The electrodeposition technique was successfully performed for homogeneous filling of mesopores of anodic alumina by nickel. XRD, EDX and HRSEM confirmed the formation of ordered nickel nanowire arrays. Magnetization reversal curves demonstrate highly anisotropic magnetic behavior of the nanocomposites. It was shown that increasing the particles diameter at constant interwire distance results in enhancement of magnetic dipole interactions and decrease of the coercive force. The polarized SANS technique in external magnetic field was first applied for characterization of the structure of ordered arrays of magnetic nanowires. This method may give extremely valuable information on the magnetic structure of ordered nanosystems excluding nonhomogeniety effects and defects of microstructure.

Acknowledgments

References

[1] S. Shingubara, J. Nanoparticle Res. 5 (2003) 17.
[2] H. Pan, B. Liu, J. Yi, C. Poh, S. Lim, J. Ding, Y. Feng, H.A. Huan, J. Lin, J. Phys. Chem. B 109 (2005) 3094.
[3] C.R. Martin, Science 266 (1994) 1961.

[4] A.K. Menon, B.K. Gupta, Nanostruct. Mater. 11 (1999) 965.

[5] O. Jessensky, F. Müller, U. Gösele, J. Electrochem. Soc. 145 (1998) 3735.

[6] K. Nielsch, J. Choi, K. Schwirn, R.B. Wehrspohn, U. Gösele, Nano Lett. 2 (2002) 677.

[7] F. Li, L. Zhang, R.M. Metzger, Chem. Mater. 10 (1998) 2470.

[8] H. Masuda, F. Hasegwa, S. Ono, J. Electron. Soc. 144 (1997) L127.

[9] R.E. Benfield, D. Grandjean, J.C. Dore, H. Esfahanian, Z. Wu, M. Kröll, M. Geerkens, G. Schmid, Faraday Discuss. 125 (2004) 327.

[10] L. Sun, Y. Hao, C.-L. Chien, P.C. Searson, IBM J. Res. Dev. 49 (2005) 79.